

# Feasibility studies for a wireless 60 GHz tracking detector readout

S. Dittmeier<sup>a,\*</sup>, A. Schöning<sup>a</sup>, H.K. Soltveit<sup>a</sup>, D. Wiedner<sup>a</sup>

<sup>a</sup>*Physikalisches Institut der Universität Heidelberg, Im Neuenheimer Feld 226, 69120 Heidelberg, Germany*

## Abstract

The amount of data produced by highly granular silicon tracking detectors in high energy physics experiments poses a major challenge to readout systems. At high collision rates, e.g. at LHC experiments, only a small fraction of data can be read out with currently used technologies. To cope with the requirements of future or upgraded experiments new data transfer techniques are required which offer high data rates at low power and low material budget.

Wireless technologies operating in the 60GHz band or at higher frequencies offer high data rates and are thus a promising upcoming alternative to conventional data transmission via electrical cables or optical fibers. Using wireless technology, the amount of cables and connectors in detectors can be significantly reduced. Tracking detectors profit most from a reduced material budget as fewer secondary particle interactions (multiple Coulomb scattering, energy loss, etc.) improve the tracking performance in general.

We present feasibility studies regarding the integration of the wireless technology at 60GHz into a silicon tracking detector. We use spare silicon strip modules of the ATLAS experiment as test samples which are measured to be opaque in the 60GHz range. The reduction of cross talk between links and the attenuation of reflections is studied. An estimate of the maximum achievable link density is given. It is shown that wireless links can be placed as close as 2cm next to each other for a layer distance of 10cm by exploiting one or several of the following measures: highly directive antennas, absorbers like graphite foam, linear polarization and frequency channeling. Combining these measures, a data rate area density of up to 11 Tb/(s · m<sup>2</sup>) seems feasible. In addition, two types of silicon sensors are tested under mm-wave irradiation in order to determine the influence of 60GHz data transmission on the detector performance: an ATLAS silicon strip sensor module and an HV-MAPS prototype for the Mu3e experiment. No deterioration of the performance of both prototypes is observed.

**Keywords:** Tracking detectors, Detector readout, Wireless readout, Data transmission, 60GHz, mm-waves

## 1. Introduction

Today's and future high energy particle physics experiments have to face high event rates in order to improve the sensitivity for Standard Model precision measurements and to increase the discovery potential for physics beyond the Standard Model. Detectors with ever-increasing granularity have to be used in order to enhance sensitivity limits due to spatial and momentum resolution. Constraints on space, material budget, power consumption and radiation hardness are nowadays the main limitation for the detector construction and the data readout bandwidth. Thus, there is an increased demand for new readout techniques that allow data transfer at extremely high rates.

Today, wired electrical and optical readout systems are used in particle detectors at colliders. Within the last decades, wireless data transmission has evolved significantly and data rates are becoming comparable with wired data links. Nonetheless, presently used wireless systems like WIFI or LTE are not suitable for particle detectors because of the limited data throughput and the large antennas. But at higher carrier frequencies a wireless detector readout seems feasible. A large

bandwidth of 9GHz provided in the 60GHz band allows data rates of several Gb/s even with simple modulation schemes. Due to the short wavelength of  $\lambda \approx 5$  mm antennas have a very small form factor.

Commercial chips for the 60GHz frequency band are available on the market, but none of them is foreseen to be used in particle physics experiments as the following requirements are usually not met: the transceiver chip has to be radiation hard; it must be operated at low power and should provide a high bandwidth at the same time. For that reason a new 60GHz transceiver ASIC for particle physics applications is currently designed [1, 2].

Wireless readout of a tracking detector for a fast track-trigger application was proposed in [3]. The authors describe how wireless readout can be exploited to transmit hit information between several highly granular silicon tracking layers to enable a fast trigger decision. The readout scheme, depicted in Figure 1, assumes a radial data transfer from the inner detector layers to the outside, thus facilitating the implementation of track finding algorithms in on-detector logic.

In this paper we present feasibility studies regarding the integration of the 60GHz wireless technology in a silicon tracking detector. Several aspects relevant for the implementation of 60GHz links are studied: transmission losses, interference effects, absorbing materials and the influence of the antenna

\*Corresponding author

Email address: dittmeier@physi.uni-heidelberg.de (S. Dittmeier)

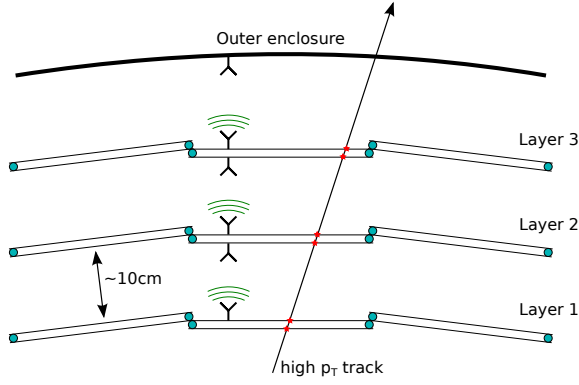


**Figure 1:** Conceptual sketch of a wireless radial readout of a cylindrical tracking detector, adapted from [3].

design. In particular, we study how wireless signals can be directed with low material horn antennas and how unwanted reflections from detector modules can be attenuated. From these studies we estimate the maximum density of wireless links that can be operated in parallel between detector layers. In addition, the influence of 60 GHz waves on a silicon pixel sensor prototype and on a silicon strip detector module is tested and it is found that the detector performance is not degraded.

## 2. 60 GHz transmission and reflection tests

In order to maximize the data throughput of a wireless readout system, as depicted in Figure 1, links have to be packed densely and the maximum possible bandwidth should be fully exploited by every single link. The main challenge is to avoid cross talk between parallel and subsequent, chained links. The latter is granted as radio signals in the 60 GHz band do not pass detector layers with metal layers implemented. A first study of transmission of mm-waves through an ATLAS SCT module [4], see Figure 2, showed that mm-waves cannot penetrate tracking detector modules [3]. We repeat this measurement with increased sensitivity and also with a different type of silicon detector modules.

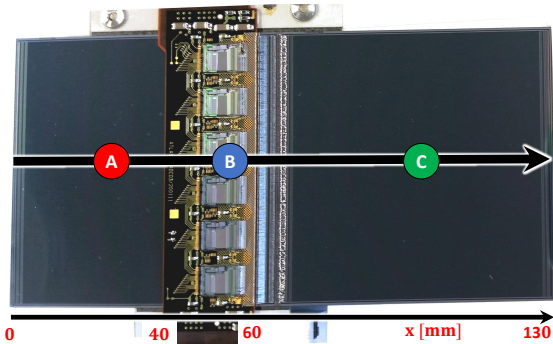


**Figure 2:** The ATLAS SCT barrel module [4] under test. Positions for frequency scans are denoted by (A), (B) and (C). A position scan is performed along the black arrow.

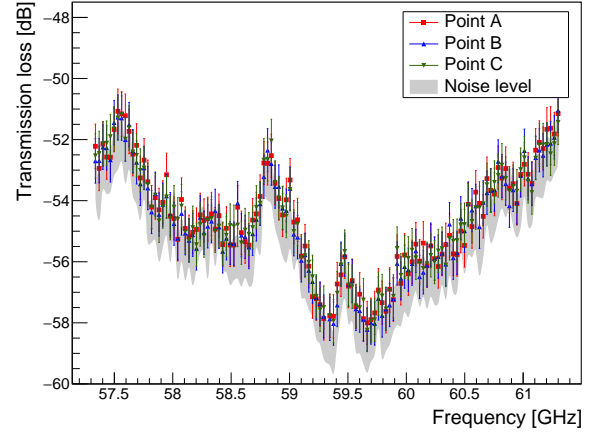


**Figure 3:** Transmission loss through the ATLAS SCT barrel module as function of the frequency at positions A, B and C (see Figure 2) and the noise limited sensitivity of the spectrum analyzer. The uncertainties of 1 dB are due to intensity variations observed with the spectrum analyzer in the power range of  $-90$  dBm.

### 2.1. Tests with an ATLAS SCT barrel module

A spare silicon strip detector module from the ATLAS barrel detector, depicted in Figure 2, is mounted on a 2D movable stage and placed in line of sight (LOS) of two horn antennas for transmission and reception. The module is irradiated with linearly polarized waves in the range from 57.3 GHz to 61.3 GHz<sup>1</sup>. The intensity transmitted through the module is measured with a spectrum analyzer in the radio frequency band without down conversion. The transmitted intensity is normalized to the intensity without module in-between. The setup is able to resolve transmission losses down to  $-55$  dB at a minimum power of about  $-90$  dBm over the frequency range mentioned above. To avoid distortions of the measurement by accidental reflections or diffraction aluminium plates and graphite foam is used as shielding.

Spectra of the transmission loss through the barrel module at positions A, B and C are shown in Figure 3 together with the noise limited sensitivity of the spectrum analyzer. The region of most interest is region B, as a 60 GHz transceiver would have to be placed on the readout electronics hybrid. Especially with highly directive antennas, most of the wireless signal intensity would be focused within this region. No transmitted signal can be measured at the positions under test, corresponding to a transmission loss of more than  $-50$  dB over the entire frequency range.

Figure 4 shows the transmission loss averaged over the chosen frequency band at various positions along the module. Again, no transmission is observed independent of the polarization of the radio signal.

<sup>1</sup>If not stated otherwise, all of the following tests are done with the HMC6000/6001 transmitter and receiver chips by Hittite [5].

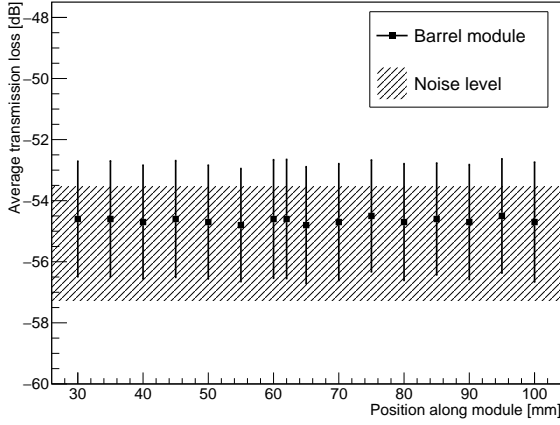


**Figure 4:** Transmission loss of the barrel module averaged over the frequency band for a position scan (along the arrow in Figure 2) and the noise limited sensitivity of the spectrum analyzer. The uncertainties represent the RMS of the average measurements.

## 2.2. Tests with an ATLAS SCT endcap module

The measurement is repeated with a spare ATLAS SCT endcap module [6], see Figure 5. A position scan is performed only in the central region to avoid diffraction at the edges. Again, the most interesting region for placing a 60 GHz transceiver is on the readout electronics hybrid, around position A in Figure 5. Figure 6 shows the transmission loss spectra for positions A, B and C on the module, compared to the measurement's sensitivity level. As expected, large variations depending on the frequency are observed in the readout electronics region due to the assembly hole and the gap between hybrid and flex print.

The frequency averaged transmission loss as function of the position on the module, see Figure 7, is  $-20\text{ dB}$  to  $-40\text{ dB}$  in the electronics region for the reasons mentioned above, while the silicon strip region is opaque for the mm-waves due to metalization.

We also measure the reflection for the endcap module normalized to the reflection at a highly reflective aluminum

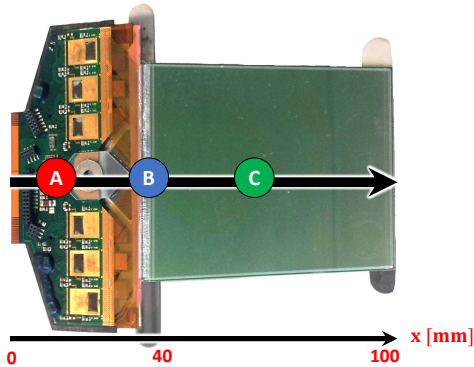


**Figure 5:** The ATLAS SCT endcap module [6] under test

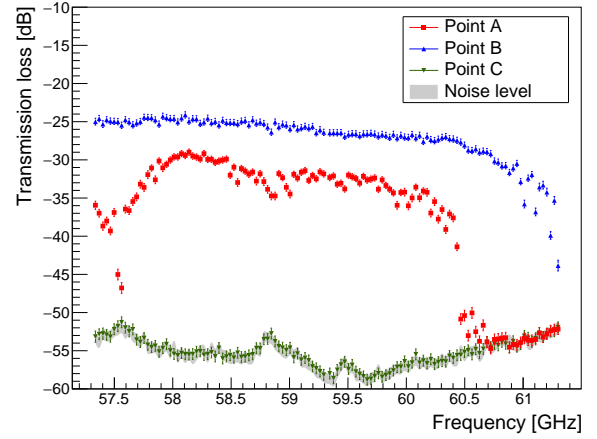


**Figure 6:** Transmission loss spectra of the endcap module at positions A, B and C (see Figure 5). The uncertainties are again due to intensity variations observed in the spectrum analyzer.

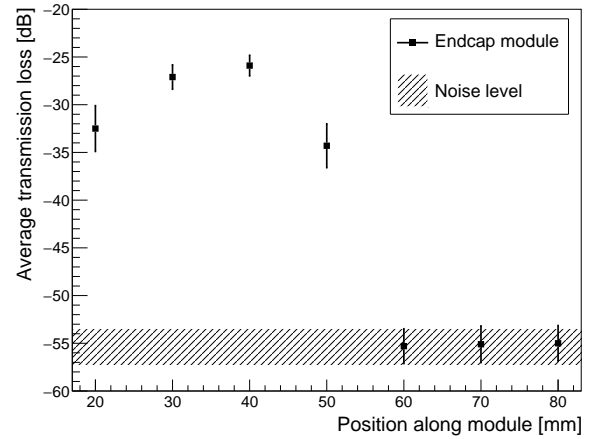


**Figure 7:** Transmission loss of the endcap module averaged over the frequency band for a position scan (along the arrow in Figure 5).

plate for reference. This measurement is performed at a fixed frequency of  $f_{RF} = 59.23\text{ GHz}$  with waves polarized perpendicularly to the incident plane. The intensity of the signal is measured under the assumption that the incident and reflected angle are identical. As can be seen in Figure 8, the strip sensor (point C) reflects the signal without any significant losses. The readout electronics hybrid (point A) and the bond wire region (point B) of the module show some reflection losses. This could be due to absorption or scattering as the module's surface is not flat in this region.

Small size components like capacitors, chips, etc. lead to scattering of 60 GHz waves. Such effects are difficult to calculate or simulate as standard ray tracing programs fail to describe the data without implementing a detailed model for diffraction [7].

Although pure silicon is not reflective, silicon detectors are

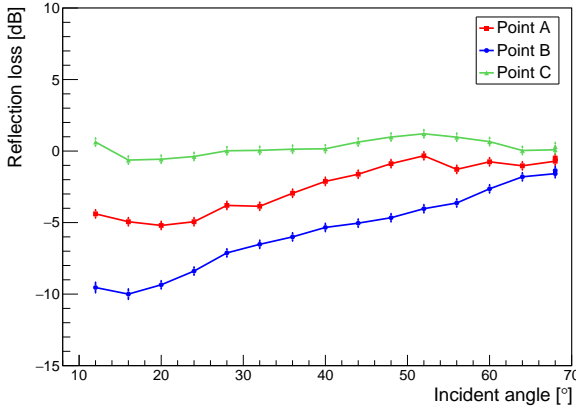


**Figure 8:** Reflection loss of the endcap module at  $f_{RF} = 59.23$  GHz at positions A, B and C (see Figure 5) as a function of the angle of incidence. The uncertainties are 0.3 dB to 0.5 dB due to intensity variations in the power range of  $-30$  dBm to  $-40$  dBm, correspondingly.

highly reflective in the 60 GHz band due to metalization and do not allow for any signal transmission through the sensor. Also parts belonging to the readout electronics, where a wireless transceiver chip and antenna would be placed, are in general reflective. Depending on the specific application, these reflections might induce cross talk. Absorbing materials could be used as shields to attenuate reflections. Gaps and not fully metalized layers, like the flex print of the endcap module, lead to transmission. Absorbing materials could be used to cover gaps and reduce inadvertent transmission. The reduction of cross talk by means of absorbing materials is further discussed in section 3.3.

### 3. Reduction of cross talk

A tracking detector represents a highly stable environment for a wireless communication system. Once it is installed, all wireless links are stationary. Therefore, a wireless readout system can be designed and optimized in such a way that interference effects between different links are minimized. However, assuming an extremely high link density, cross talk can be an issue. There are several measures which can also be combined to reduce cross talk, if necessary. First of all, one can use directive antennas with high gain and small beamwidth. By increasing the gain of the antenna the transmitted power can be decreased while keeping the signal over noise ratio (S/N) in the receiver constant. Secondly, one can exploit linear polarization. By using orthogonal polarization states cross talk between adjacent links can be largely reduced. Thirdly, reflections can be attenuated by means of absorbing materials. Low mass materials with high absorbance might be preferably used in order not to increase the material budget. Fourthly, the frequency band can be divided in different channels, using a tunable VCO with sharp filters or low bandwidth antennas.

Studies on cross talk suppression methods are described in detail in [8]. Here a summary of these results for the first

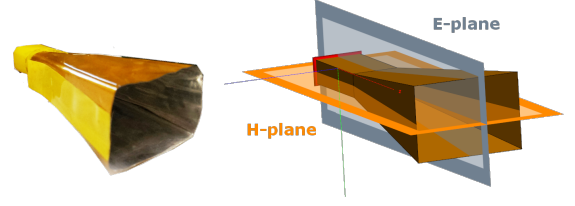


**Figure 9:** Left: photograph of a 3.5 cm long horn antenna made from an aluminum and Kapton<sup>®</sup> foil laminate. Right: the H-plane is spanned by the long edge and the direction of emittance (orange plane); the E-plane is spanned by the short edge and the direction of emittance (grey plane).

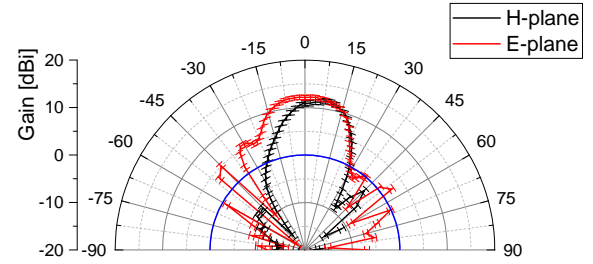


**Figure 10:** Measured polar radiation pattern in the E- and H-plane of a tested Al-Kapton<sup>®</sup> horn antenna at  $f = 60.85$  GHz. The blue line represents an isotropic emitter with  $G = 0$  dBi.

three options is given. Frequency channeling is discussed in section 4.4 in the context of bit error rate measurements.

#### 3.1. Directive antennas

Requirements on antennas are highly application specific. Flat patch antennas have a small form factor and can offer high gain and directivity if several patches are combined and interfere constructively. However, their bandwidth is typically limited to less than 1 GHz [9]. Other antenna types as slot antennas [10] or Vivaldi antennas [11] offer higher bandwidths. Due to the small form factor, it is also possible to integrate antennas on-chip. But because of losses in the silicon substrate, these antennas usually have a reduced radiation efficiency [12].

For high bandwidth applications horn antennas are a good alternative which, however, require some space. To be usable in the active volume of a tracking detector, the antenna should consist of as little material as possible. As an alternative to commercial brass antennas we produced horn antennas from a 25  $\mu$ m aluminium and 25  $\mu$ m Kapton<sup>®</sup> foil laminate, see Figure 9. These light weight antennas serve as a first demonstrator and are used in the following measurements. In principle, the aluminium could be even thinner: a 25  $\mu$ m Kapton<sup>®</sup> foil with a 50 nm thin aluminium layer is tested to be fully reflective at 60 GHz. Thus, horn antennas could be produced with extremely small material budget [8].

Figure 10 shows the gain of a 3.5 cm long Al-Kapton<sup>®</sup> horn antenna in the H- and E-plane measured in the far field. The



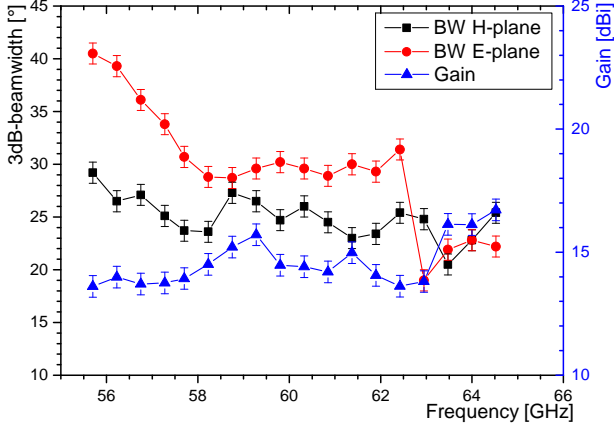


**Figure 11:** Measured beamwidth and gain of the Al-Kapton<sup>®</sup> horn antenna, shown in Figure 9.

3dB-beamwidth  $BW_{3dB}$  is derived to be about  $25^\circ$  in the H-plane and  $30^\circ$  in the E-plane. A scan of the beamwidth and forward gain is performed in the frequency range from 55 GHz to 65 GHz, see Figure 11. In the whole range a gain  $G \geq 13$  dBi is achieved.  $BW_{3dB}$  decreases accordingly in both planes as more intensity is focused in the forward direction. The errors on gain and beamwidth are derived from the following uncertainties: variations of the transmitted power over time, variations of signal attenuation along the coaxial cables due to bending, and geometrical uncertainties on the angle.

The horn antennas presented here show high gain and high directivity. They can be made of very little material such that they amount to less than 0.1% of a radiation length. A drawback is their volume making the mechanical integration into a particle detector experiment potentially difficult. It should further be noted that horn antennas require a primary feed antenna, for instance a single wideband patch or dipole antenna.

### 3.2. Polarization

Transmission tests with horn antennas with linearly polarized waves are performed and the polarization suppression factor PSF between orthogonal polarization states,

$$\text{PSF} = \frac{|\vec{P}_{act} \times \vec{P}_{nom}|}{|\vec{P}_{act} \cdot \vec{P}_{nom}|}, \quad (1)$$

is measured. Here are  $\vec{P}_{nom}$  the nominal polarization vector of the antenna and  $\vec{P}_{act}$  the measured polarization vector. The distance between the antennas' apertures is about 7.5 cm. Two industrially produced brass horn antennas serve as reference. Results are shown in Table 1.

Compared to the brass antennas, the polarization suppression of the Al-Kapton<sup>®</sup> horns is smaller due to the shorter length and mechanical imperfections. Despite these imperfections, pickup of signals from orthogonal polarization states is suppressed by more than 10 dB.

Horn antenna 1 Transmitter	Horn antenna 2 Receiver	PSF [dB]
Brass	Brass	$-53.0 \pm 1.0$
4.5 cm Al-Kapton <sup>®</sup>	Brass	$-33.2 \pm 0.6$
3.5 cm Al-Kapton <sup>®</sup>	Brass	$-14.8 \pm 0.4$
3.5 cm Al-Kapton <sup>®</sup>	4.5 cm Al-Kapton <sup>®</sup>	$-13.5 \pm 0.4$

**Table 1:** Polarization suppression factor (PSF) of orthogonal polarization states using different antennas. Uncertainties are derived from measured intensity variations.

### 3.3. Absorption and reflections

Absorbing materials are in particular useful to avoid transmission through gaps in the detector and to attenuate reflections from detector modules. We tested different types and thicknesses of low density carbon impregnated foams, which are commonly used as absorber for other microwave applications. A list of the producer's material label (by ARC Technologies), the corresponding thickness and its density can be found in Table 2. All tested foams are of very low density and have large radiation lengths estimated to be 6 m to 9 m. For foam thicknesses of 1 cm or less, the contribution to the material budget of standard silicon detectors is rather small with  $X/X_0 \lesssim 1\%$ .

The foam samples are placed between two antennas to measure the transmission and reflection. The transmitted intensity is normalized to the intensity measured in LOS configuration.

As the pore size of the foam is well below the signal wavelength of  $\lambda \approx 5$  mm, the surface of the foam can be treated as a plane surface. Transmission and reflection including polarization are described by the Fresnel equations [15]. The transmission loss  $T$  through a layer of foam with a finite thickness  $d$  is the product of the transmission losses at both surfaces and the absorption loss inside the foam described by the Beer-Lambert law:

$$T_{\perp/\parallel} = |t_{\perp/\parallel}(\alpha, \beta, N_1, N_2)|^2 \cdot |t_{\perp/\parallel}(\beta, \alpha, N_2, N_1)|^2 \cdot e^{-ad}, \quad (2)$$

Foam	$d$ [mm]	$\rho$ [mg/cm <sup>3</sup> ]	$a$ [dB/cm]
LS-11451-1	6.35	$73.8 \pm 0.7$	$27.3 \pm 0.2$
LS-10122-9 [13]	12.70	$54.0 \pm 1.0$	$12.8 \pm 0.1$
LS-11297-1	19.05	$58.8 \pm 0.5$	$24.1 \pm 1.4$
LS-10640-1 [14]	25.40	$50.7 \pm 0.5$	$19.5 \pm 0.1$

**Table 2:** Properties of the tested graphite foams: thickness  $d$  (from ARC Technologies), density  $\rho$  and absorption loss  $a$  at  $f = 60.7$  GHz (measured).

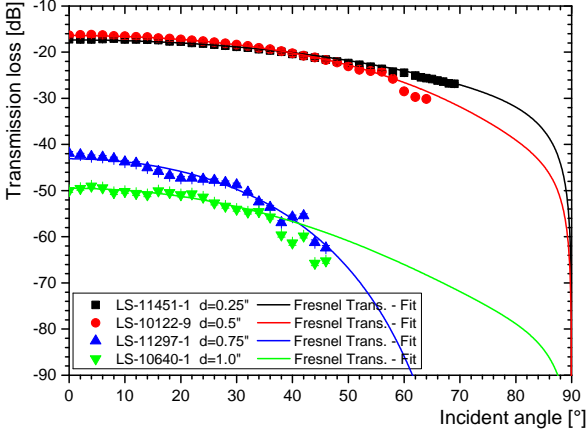


**Figure 12:** Transmission loss of graphite foam samples at  $f = 60.7\text{GHz}$  for perpendicularly polarized waves. The uncertainties of  $0.2 - 1.0\text{dB}$  are due to intensity variations in the transmitted signal and the noise limited sensitivity of the spectrum analyzer. A fit of Equation 2 is applied to all four data sets.

with the polarization dependent transmission loss

$$t_{\perp}(\alpha, \beta, N_1, N_2) = \frac{2N_1 \cos \alpha}{N_1 \cos \alpha + N_2 \cos \beta}, \quad (3)$$

$$t_{\parallel}(\alpha, \beta, N_1, N_2) = \frac{2N_1 \cos \alpha}{N_2 \cos \alpha + N_1 \cos \beta}, \quad (4)$$

for waves polarized perpendicularly and parallel to the incident plane, respectively. The incident and the refracted angle are denoted by  $\alpha$  and  $\beta$  and the complex index of refraction  $N_i$  is defined as

$$N_i = n_i - i\kappa_i. \quad (5)$$

Here,  $N_1 = 1$  for air and  $N_2$  is the index of refraction of the graphite foam under test. The absorption coefficient  $a$  is related to the imaginary part of the refractive index and the vacuum wavelength  $\lambda_0 \approx 5\text{mm}$ :

$$a = \frac{4\pi\kappa}{\lambda_0}. \quad (6)$$

Figure 12 shows the measured transmission loss of the foam samples as function of the incident angle. All samples attenuate the transmitted signal by at least  $15 \pm 1\text{dB}$  over the whole angular range. A  $\chi^2$ -fit of Equation 2 is used to derive the absorption coefficient  $a$ . Results are given in Table 2 in units of  $\text{dB/cm}$ . All samples show an absorption coefficient of  $20\text{dB/cm}$  and higher, except foam LS-10122-9. Foam LS-11451-1 shows the highest absorption and therefore the best performance.

Similarly, absorption is measured over a larger frequency range in the  $60\text{GHz}$  band. No significant dependence on the frequency is found. In addition, the homogeneity of the absorber materials is studied. A large piece of foam is used to

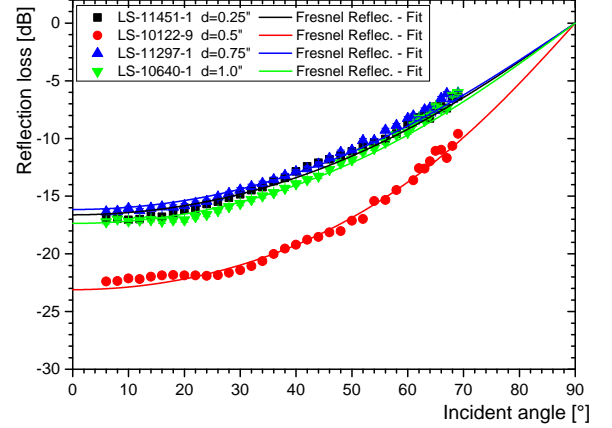


**Figure 13:** Reflection loss of graphite foam samples at  $f = 60.7\text{GHz}$  for perpendicular polarized waves. The uncertainties due to intensity variations are  $0.2 - 0.3\text{dB}$ . A fit of Equation 7 is applied to all four data sets.

study the fluctuations in the absorption coefficient  $a$  across the sample and variations up to  $3\text{dB/cm}$  are measured. Fluctuations could be due to inhomogeneities in the thickness, porosity and impregnation with graphite.

Similar to the transmission, the reflection loss  $R$  is described by

$$R_{\perp/\parallel} = |r_{\perp/\parallel}|^2, \quad (7)$$

with

$$r_{\perp} = \frac{N_1 \cos \alpha - N_2 \cos \beta}{N_1 \cos \alpha + N_2 \cos \beta}, \quad (8)$$

$$r_{\parallel} = \frac{N_2 \cos \alpha - N_1 \cos \beta}{N_2 \cos \alpha + N_1 \cos \beta}, \quad (9)$$

for perpendicular and parallel polarization.

The reflected intensity is measured and normalized to the power reflected by an aluminium plate. Figure 13 shows the reflection loss of the four foam samples at a frequency of  $f = 60.7\text{GHz}$  with waves polarized perpendicularly to the incident plane. The data is well fitted by the Fresnel ansatz. All samples show a reflection loss below  $-10\text{dB}$  up to large incident angles. The second thinnest sample, foam LS-10122-9 (red curve), shows a significantly lower reflected intensity than the other samples. The measurement presented is repeated with the foam glued onto an aluminium plate and no difference is found. We conclude that, due to the high absorption coefficient of the foam, the total reflection loss is dominated by the first air - graphite foam transition.

The methods discussed here are well suited to reduce reflections and cross talk in tracking detectors without stressing the material budget. For example, inadvertent transmission through gaps as observed for the endcap module in section 2 can be easily damped by more than  $20\text{dB}$  with a layer of graphite foam

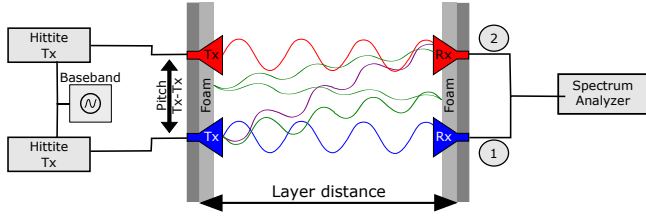


**Figure 14:** Sketch of the setup to measure cross talk with two links between highly reflective aluminium layers. LOS cross talk is indicated as purple wave.

as thin as 1 cm, corresponding to about 0.1 - 0.2 % of a radiation length. Reflections from detector modules and electronic components can be attenuated up to large incident angles by 10 dB and more by covering them with a layer of graphite foam.

#### 4. Link density studies

By combining the different methods for reducing cross talk discussed in the previous section, we study experimentally how close two parallel 60 GHz links can be placed without disturbing each other, see Figure 14. We define as S/N the ratio of the signals from transmitter #1 over transmitter #2 measured with the spectrum analyzer via the antenna of receiver #1.

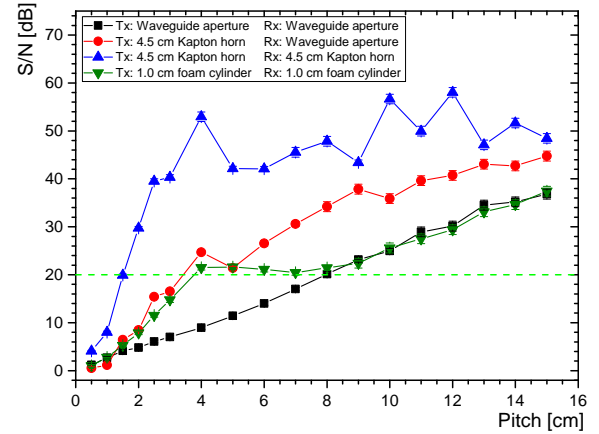
We define the link quality to be sufficient for an S/N of 20 dB or higher. This value corresponds to a theoretical bit error rate of  $10^{-12}$ , or lower, for many modulation schemes, e.g. On-Off-Keying.

##### 4.1. Line of sight cross talk

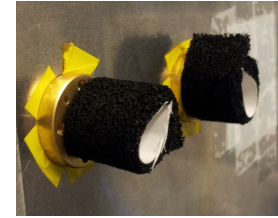
As LOS cross talk we define signals transmitted directly across different transmitter-receiver pairs. To study LOS cross talk, transmitters and receivers are placed in air without reflecting layers behind the antennas. The S/N is measured as function of the pitch, defined as the distance between the two transmitters. The distance between transmitters and receivers is fixed to 10 cm without antennas and both links have identical polarization.

Figure 15 shows the S/N for different setups. For reference, non-directive waveguide apertures are used ( $BW_{3dB} \approx 75^\circ$ ), for which the S/N increases linearly as function of the pitch. Without any measures a minimum pitch of about 8 cm is necessary to achieve an S/N of 20 dB. Using highly directive Al-Kapton<sup>®</sup> horn antennas reduces the transmission distance in air to 6.5 cm and 3 cm for one or two antennas, respectively. With one antenna on the transmitting or receiving side, the minimum pitch is reduced to 4 cm. With Al-Kapton<sup>®</sup> horn antennas installed on both sides, links can be placed as close as 2 cm next to each other without significant interference effects. Variations in the S/N with both horn antennas at pitches larger than 4 cm are most likely due to the irregular radiation pattern in the side lobes (see Figure 10).

Without using any directive antennas cross talk can be reduced just by absorber shields. For a test, all transmitters and



**Figure 15:** S/N in the radio frequency spectrum with LOS induced cross talk as function of the antenna pitch for different setups.



**Figure 16:** 1 cm long hollow graphite foam cylinders shielding two wireless links. The paper covering the adhesive on the inside of the cylinder was tested to not affect the signal.

receivers are equipped with 1 cm long, hollow graphite foam cylinders on top of the waveguide apertures to shield lateral radiation (see Figure 16). It is found that shielded links can be placed as close as 4 cm next to each other to fulfill our S/N requirement. For small pitch values, the absorber shielding was found to be as effective for cross talk reduction as horn antennas on one side. For larger pitch, there seems to be no benefit from using shields. This could be due to rather strong side lobes generated by the cylinder's aperture. All results in Figure 15 are found by studying cross talk in the H-plane. Similar results are obtained in the E-plane [8].

##### 4.2. Bit error rate tests

For data transmission applications bit error rates (BER) give the relevant figure of merit. Again, two links are placed at variable pitch with a fixed distance of 10 cm between transmitter and receiver, not including the size of any antennas. The BER is measured for a data rate of 1.76 Gb/s using Minimum Shift Keying (MSK) as modulation scheme. Both links use the same polarization state and the same carrier frequency.

BER measurements are performed with different configurations: horn antennas for transmitters only, horn antennas for transmitters and receivers, and 1 cm long hollow graphite foam

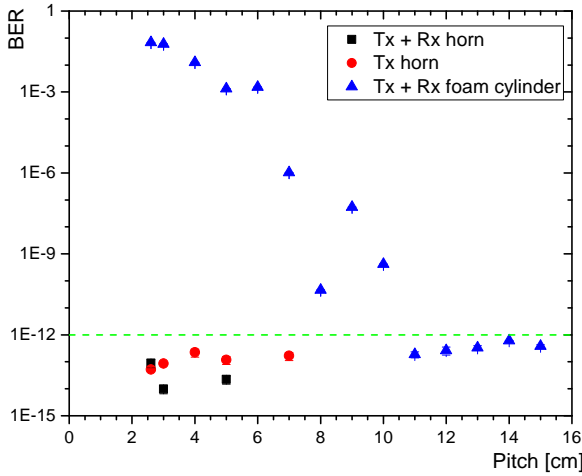


**Figure 17:** Influence of LOS cross talk on the bit error rate of a wireless data transmission, shown as function of the pitch between two parallel links. Distance between transmitter and receiver is set to 10cm. Both links are operated at the same carrier frequency.

cylinders as shields instead of antennas. The BER results are shown in Figure 17 as function of the pitch. With horn antennas bit error rates smaller than  $10^{-12}$  are achieved for all studied pitches. Even with foam shields only, bit error rates below  $10^{-12}$  are achieved for a pitch larger than 10cm. Large variations below a pitch of 10cm are likely due to side lobes in the radiation pattern generated by the cylinder.

#### 4.3. Cross talk due to reflections

Silicon detector modules are highly reflective as discussed in Section 2. In a real tracking detector 60GHz radiation is reflected between the silicon detector layers which leads to cross talk. By enclosing the volume with aluminium plates, the silicon detector environment is emulated, see Figure 14. Two links are mounted through holes in each of the aluminium layers facing at a distance of 10cm. The pitch between the links is set to 5cm, 10cm and 15cm. Different configurations with directive horn antennas, graphite foam shields stuck onto the aluminium layers and orthogonal polarization states are tested. Again, waveguide apertures are used as non-directive reference antennas. The transmission distance in air is reduced to 6.5cm and 3cm when one or two horn antennas are applied, respectively.

Results of various measurements performed with this setup are shown in Figure 18. All antenna setups are measured with both polarization states (parallel and orthogonal) between the two links. We find that at a pitch of 15cm all studied setups give a satisfying S/N. For a pitch of 10cm only the reference measurement with parallel polarization fails the S/N criterion. With directive antennas stable data transmission at a pitch of 5cm is possible for all studied configurations. Using orthogonal

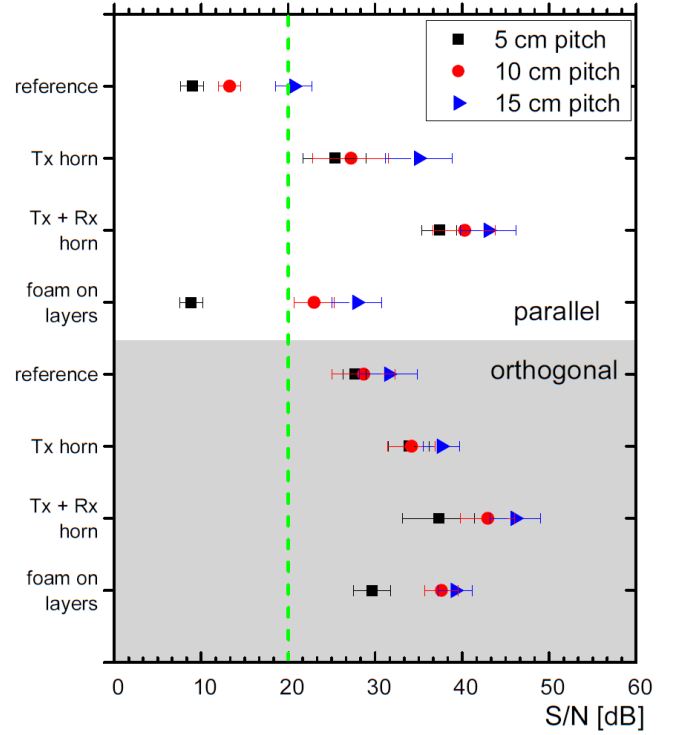


**Figure 18:** S/N for two parallel links operated between two fully reflective aluminium layers at a distance of 10cm. Results are shown for parallel polarization states (top, white background) and orthogonal polarization states (bottom, grey background).

polarization for neighboring links, a good S/N is obtained for all tested setups even without directive antennas and a pitch of 5cm or less seems to be feasible. By combining directive antennas and absorbing foam the S/N ratio can be increased further. The operation of 60GHz links between highly reflective materials is possible even at a small pitch if directive antennas, absorber materials and/or polarization are exploited.

#### 4.4. Frequency channeling

The carrier frequency of the Hittite transmitter chip is tunable which allows to use frequency channeling. To measure quantitatively the BER as function of the carrier offset, two parallel links are positioned at a pitch of 2.6cm using the same polarization state. Foam cylinders on top of the waveguide apertures are used for minimum shielding. The carrier frequency offset is varied in steps of 500MHz.

The results are shown in Figure 19. For frequency offsets smaller than the chipset's bandwidth ( $\pm 1.8$ GHz) a plateau with a BER of a few percent is visible. With increasing offset the BER decreases and reaches  $10^{-10}$  for an offset larger than twice the bandwidth. With this setup, the usage of 3 frequency channels in parallel within the full 60GHz band seems possible. In order to actually benefit from channeling, filters with very sharp cutoff frequencies are required.

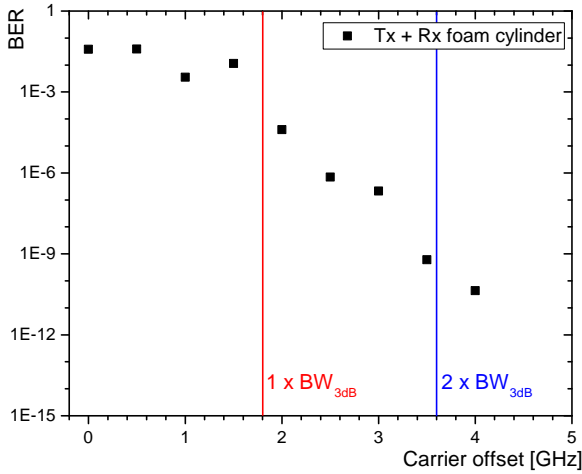


**Figure 19:** Measured bit error rates of two parallel operated links at a pitch of 2.6cm as function of the carrier frequency offset. The links are operated with minimum shift keying at up to 1.76Gbps. No directive antennas are applied. The 3dB-bandwidth of the Hitite transceivers (1.8GHz) is indicated as red line, twice the bandwidth as a blue line.

#### 4.5. Achievable link density

From the results presented in this section, we can give an estimate on the possible link density. For this, we assume a tracking detector environment with distances of 10cm between layers and a minimum pitch of 3.5cm between links. We first assume On-Off-Keying (OOK) as modulation scheme with a spectral efficiency of  $\rho_{\text{OOK}} \approx 0.5 \text{ b/s/Hz}$ . Using the full 9 GHz bandwidth per channel yields a data rate of 4.5Gb/s per link. The resulting data rate area density is about  $3.7 \text{ Tb}/(\text{s} \cdot \text{m}^2)$ .

A higher order modulation scheme can increase the spectral efficiency. MSK, providing  $\rho_{\text{MSK}} = 1 \text{ b/s/Hz}$ , would be a viable candidate, as it can still be demodulated non-coherently. Using the same bandwidth we estimate that a data rate area density of about  $7.3 \text{ Tb}/(\text{s} \cdot \text{m}^2)$  is feasible.

Exploiting frequency channeling, the link density can be further increased and we assume a minimum pitch of 2cm. With an even higher order modulation scheme, three frequency channels with data rates of 4.5 Gb/s per channel seem feasible. This results in a data rate area density of around  $11 \text{ Tb}/(\text{s} \cdot \text{m}^2)$ . However, frequency channeling and higher order modulation schemes typically come at the cost of increased complexity and power consumption.

#### 5. Pickup of 60 GHz noise

Deterioration of the detector performance due to pickup of noise from 60GHz communication is a potential worry for the operation of wireless links inside the detector. However, cut-off frequencies of sensors and readout chips for silicon

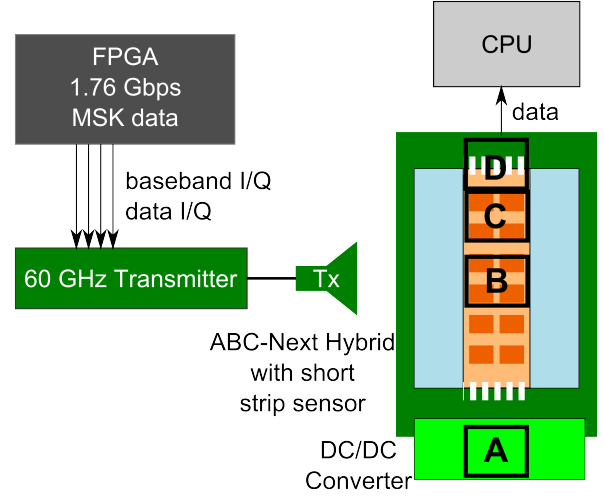


**Figure 20:** Block diagram of the setup used for the irradiation test at Freiburg. A, B, C and D indicate different antenna positions used in the test. The 12 readout chips are illustrated as brown boxes on the orange readout hybrid.

detectors are typically below a few GHz. Therefore, no interference between the 60GHz links and tracking detector modules is expected. To demonstrate this, 60GHz irradiation tests are performed for different silicon strip and pixel detectors.

#### 5.1. Test with silicon strip sensor prototypes

Two ABCN endcap electronics hybrid prototypes for the phase-2 upgrade of the silicon tracking detector for the ATLAS experiment [16, 17] are tested using a teststand at the University of Freiburg which is described in [18]. One is a bare electronics hybrid, while the other one is connected to short silicon strip sensors with a strip length of 2.4cm. Each prototype comprises 12 fully functional ABCN readout chips [19].

The noise level of each readout channel is measured with a threshold scan using calibrated injected charges in units of equivalent noise charges (ENC). Then, noise measurements are performed for each channel of the readout ASICs under wireless irradiation. Our 60GHz setup is used to irradiate the hybrid module using a 20dBi horn antenna from a distance of 1cm. The 60GHz transmission power is about  $-1.0 \pm 1.0 \text{ dBm}$ . A block diagram and a photograph of the test setup are shown in Figure 20 and 21, correspondingly. Four different positions are irradiated as indicated in Figure 20: (A) the power converter, (B) and (C) the readout chips, and (D) the bonding wires. The irradiation measurements are performed with carrier frequencies of 57 GHz, 60 GHz and 63 GHz.

The noise level distribution of a reference measurement and a measurement with 60GHz irradiation are shown in Figure 22 for the electronics hybrid without silicon strips. The noise distributions, see Figure 22, are compatible with each other and no significant differences are found in the mean and width of the distributions. Therefore, we set an upper limit of 1 ENC at a 95% confidence level on the increase of the average noise. Likewise, we do not observe any significant increase for the



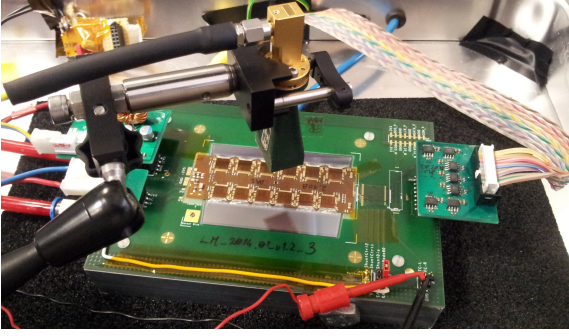


**Figure 21:** A prototype for the ATLAS endcap tracking detector upgrade [17] under irradiation of mm-waves.

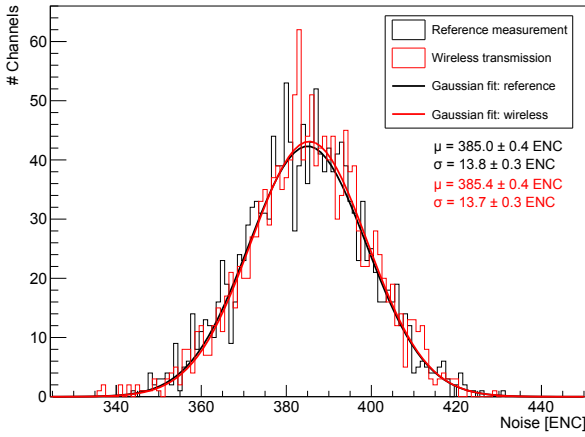


**Figure 22:** Noise distribution of all channels of the 12 ABCN readout chips without strip sensors under irradiation. The reference measurement was performed without 60GHz irradiation. Mean  $\mu$  and width  $\sigma$  of the Gaussian fits are given. No significant difference is observed.

second prototype connected to silicon strips (average reference noise level:  $570 \pm 1$  ENC; average noise with wireless irradiation:  $571 \pm 1$  ENC). Thus, we set an upper limit of 2 ENC at a 95 % confidence level on the average noise increase.

No significant rise in the noise level of the readout channels is observed at any carrier frequency or irradiated position. As expected, no influence of the wireless signal on the noise level is found.

### 5.2. Test with HV-MAPS

We performed a similar measurement with a High Voltage-Monolithic Active Pixel Sensor (HV-MAPS) [20] prototype for the Mu3e experiment [21], called MuPix [22, 23]. A picture of the 60GHz irradiation setup is shown in Figure 23. In order to see the influence of the wireless on the sensor operation, a threshold scan is performed with an  $^{55}\text{Fe}$  source, see Figure 24.

Up to a threshold of about 0.9 V the hit rate is dominated by noise. The S-curve response of the pixels to the iron source is clearly visible and has its turning point around 0.96 V with a tail to higher signals. No effect of the 60GHz irradiation on the

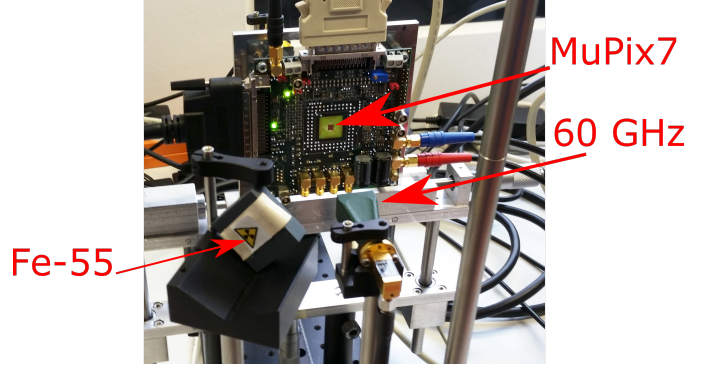


**Figure 23:** The MuPix7 HV-MAPS prototype for the Mu3e experiment in the test setup irradiated with an  $^{55}\text{Fe}$  source. The wireless signal is transmitted using a horn antenna at a distance of about 8 cm to the sensor.

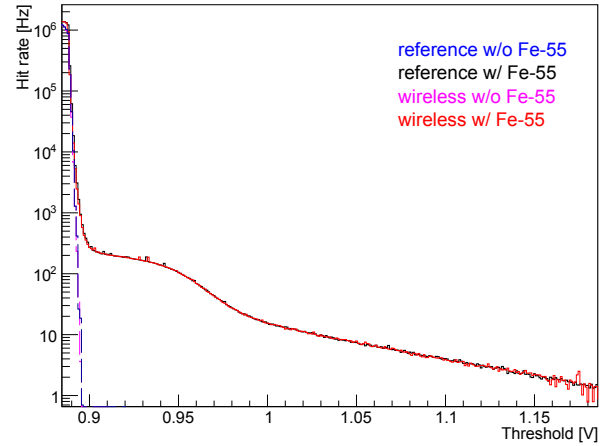


**Figure 24:** Response of MuPix7 pixels to an iron  $^{55}\text{Fe}$  x-ray source measured with a threshold scan.

sensor performance is visible. Also, no influence on the power consumption of the sensor is found. From these measurements, we can conclude that a wireless data transmission in the 60GHz band is safe with respect to the operation and performance of current silicon tracking detector sensors.

## 6. Conclusion

The feasibility of a wireless readout system for a tracking detector was studied. Currently used ATLAS silicon strip modules are opaque to 60GHz radiation which allows to use the same carrier frequencies for communication between different, hermetically separated detector layers. It was demonstrated, using hybrid silicon strip modules from ATLAS and High Voltage-Monolithic Active Pixel Sensors (HV-MAPS) from Mu3e, that the performance of silicon detectors is not degraded under 60GHz irradiation.

By using directive antennas cross talk between neighboring links can be significantly reduced. Hence, high link densities

are possible. In addition, by exploiting linear polarization, links can be placed safely as close as 2 cm to 5 cm from each other for layer distances of 10 cm. Reflections and also transmission can be significantly attenuated using graphite foam, which would add only about 1 % of a radiation length to the material budget due to the low density. The contribution of antennas to the material budget is also very small if patch or horn antennas made of thin metalized foils are used. Frequency channeling is another option to decrease cross talk, but at the expense of a reduced bandwidth per link. With all these measures combined we estimate that a data rate area density of 11 Tb/(s · m<sup>2</sup>) is feasible for a 60 GHz wireless readout system. The study demonstrated that the 60 GHz wireless technology is a very attractive alternative to wired and optical readout systems for future detector applications.

## Acknowledgments

S. Dittmeier acknowledges support by the *International Max Planck Research School for Precision Tests of Fundamental Symmetries*. The authors would like to thank S. Kühn and U. Parzefall (University of Freiburg) for the opportunity to perform measurements with ATLAS SCT endcap modules. Furthermore, the authors would like to express their gratitude to R. Brenner (University of Uppsala) for discussions and the supply of a spare ATLAS SCT barrel module.

## References

- [1] H.K. Soltveit, S. Dittmeier, A. Schöning and D. Wiedner, “Towards Multi-Gigabit readout at 60 GHz for the ATLAS silicon microstrip detector”, Nuclear Science Symposium and Medical Imaging Conference (NSS/MIC), 2013 IEEE, pages 1–6, 2013.
- [2] H.K. Soltveit, R. Brenner, A. Schöning and D. Wiedner, “Multi-Gigabit Wireless data transfer at 60 GHz”, JINST, **7** C12016, 2012.
- [3] R. Brenner and S. Cheng, “Multigigabit wireless transfer of trigger data through millimetre wave technology”, JINST, **5** C07002, 2010.
- [4] T. Kondo et al., “Construction and performance of the ATLAS silicon microstrip barrel modules”, Nucl. Instrum. Meth., **A485** 27–42, 2002.
- [5] Hitite Microwave Corporation, “HMC6000 Millimeterwave Transmitter IC”, Data sheet.
- [6] L. Feld, “Detector modules for the ATLAS SCT endcaps”, Nucl. Instrum. Meth., **A511** 183–186, 2003.
- [7] T. Hugle, “Simulation von Datenübertragung und Beugung mit einem Raytracer”, Ruprecht-Karls-Universität Heidelberg, BSc thesis, 02 2013.
- [8] S. Dittmeier, “Development of a test setup for a 60 GHz wireless transceiver for the ATLAS tracker readout”, Ruprecht-Karls-Universität Heidelberg, MSc thesis, 2013.
- [9] D. Pelikan, N. Borgefors, R. Brenner, D. Dancila and L. Gustafsson, “Wireless data transfer with mm-waves for future tracking detectors”, JINST, **9** C11008, 2014.
- [10] F. Ohnimus, I. Ndip, S. Guttowski and H. Reichl, “An efficient and broadband slot antenna for 60 GHz wireless applications”, Electrical Design of Advanced Packaging and Systems Symposium, pages 69–72, 2008.
- [11] K. Pitra, Z. Raida and J. Bartyzal, “Antenna Structures for Emerging Frequency Bands”, 18th Telecommunications forum TELFOR 2010.
- [12] K.-K. Huang and D.D. Wentzloff, “60 GHz on-chip patch antenna integrated in a 0.13-μm CMOS technology”, IEEE International Conference on Ultra-Wideband (ICUWB), pages 1–4, 2010.
- [13] ARC Technologies, “LS-10122”, Data sheet.
- [14] ARC Technologies, “LS-10640”, Data sheet.
- [15] E. Hecht, *Optics*. Addison-Wesley, 2nd edition, 1987.
- [16] K. Mahboubi et al., “The front-end hybrid for the ATLAS HL-LHC silicon strip tracker”, JINST, **9** C02027, 2014.
- [17] M. Aliev et al., “A forward silicon strip system for the ATLAS HL-LHC upgrade”, Nuclear Instruments and Methods in Physics Research Section A: Accelerators, Spectrometers, Detectors and Associated Equipment, **730** 210 – 214, 2013.
- [18] S. Kühn, “Untersuchung der Strahlenhärte von Siliziumsensoren mit einer Betaquelle”, Albert-Ludwigs-Universität Freiburg, Diploma thesis, 2006.
- [19] J. Kaplon et al., “The ABCN front-end chip for ATLAS inner detector upgrade”, Electronics for particle physics. Proceedings, Topical Workshop, TWEPP-08, pages 116–120, 2008.
- [20] I. Perić, “A novel monolithic pixelated particle detector implemented in high-voltage CMOS technology”, Nucl. Instrum. Meth., **A582** 876, 2007.
- [21] A. Blondel et al., “Research Proposal for an Experiment to Search for the Decay  $\mu \rightarrow eee$ ”, ArXiv e-prints, January 2013.
- [22] H. Augustin et al., “The MuPix high voltage monolithic active pixel sensor for the Mu3e experiment”, JINST, **10**(03) C03044, 2015.
- [23] H. Augustin et al., “The MuPix System-on-Chip for the Mu3e Experiment”, arXiv:1603.08751, 2016.